Nigerian Journal of Science and Environment 2024 Volume 22 (3) 74 – 90 ISSN: 3043 – 4440
https://doi.org/10.61448/njse223246

Analyzing the structural, optoelectronic, and optical properties of ZrS nanostructured material by adding silver (Ag) dopant to its lattice.

Shaka, O. S[1], Olisenekwu, C.[1], Ikhioya, I. L[2,3]*
[1]Department of Science Laboratory Technology, Delta State University, Abraka. Delta State
[2] Department of Physics, Faculty of Science, Federal University Lokoja, Nigeria
[3]Department of Physics and Astronomy, University of Nigeria, Nsukka, 410001, Enugu State, Nigeria
*Corresponding author's e-mail address: imosobomeh.ikhioya@unn.edu.ng

Abstract

In this study, a range of (0.01-0.03) mol was used to synthesize silver doped ZrS through electrodeposition. A three-electrode system was employed in the synthesis. Platinum is used for the anode, silver and silver chloride (Ag/AgCl) are used for the reference electrode, and FTO (fluorine-doped tin oxide) is used for the cathode. The ZrS and Ag/ZrS XRD patterns showed the materials are polycrystalline with distinct phase orientation planes. An intense peak, indexed at (111) and showing values between 23.59^o and 62.62^o, displays a heavily dampened peak plane at (111). The micrograph of the ZrS material shows a presence of hexagonal structure material along with precipitate. The presence of various silver concentrations results in particle clumping and a uniformly coated substrate surface. In the visible region, the Ag/ZrS material displays a distinct absorption band, which is attributed to the silver surface plasmon resonance. The wavelength of the surface plasmon resonance band is determined by the size, shape, and dielectric properties of the silver material and the surrounding ZrS material. The energy band structure of ZrS increases from 2.32 to 2.51 eV with increasing silver molarity due to silver incorporation within the ZrS lattice.

Keyword: X-ray diffraction patterns, optoelectronic, Energy dispersive X-ray, bandgap, Scanning electron microscopy, optical,

Introduction

The primary global challenges arising from pollution and the greenhouse effect due to fossil fuel combustion rather than renewable energy utilization are energy and environmental issues (Alzoubi *et al.*, 2021; Elhalim *et al.*, 2021). To combat the surge in energy consumption resulting from population growth and developing nations' demands, we must replace non-renewable energy sources. Finding clean and sustainable renewable energy sources is now an urgent priority (Alnehia *et al.*, 2023; Article, 2024; Bencherif *et al.*, 2022; Bouarissa *et al.*, 2021). Solar energy is considered by researchers as a cost-effective and renewable option with abundant availability and high output efficiencies. The solar photovoltaic industry relies heavily on the distribution and intensity of solar radiation. Solar thermal applications use solar energy as a heat or electricity source in technologies like concentrated fuel cells and

solar power plants (Hasan *et al.*, 2023; Ikhioya, 2024; Ikhioya and Nkele, 2024).All technologies harness sunlight and convert it into different forms. Solar energy can be converted into solar fuel through photosynthesis, as an example. Through photosynthesis, plants store solar energy by producing protons and electrons, which can be transformed into H_2 and CH_4. Biomass photosynthesis only uses 11% of solar energy. Photovoltaics convert photons into electrons for electricity, while solar thermal applications absorb and convert photons into heat(Jimin Shang *et al*., 2019; Kashif *et al.*, 2022s; Kumar *et al.*, 2016; Li *et al.*, 2019; Mattinen *et al.*, 2019). The heat is used to warm a working fluid, which can then be collected and used to directly heat spaces and water. However, the energy conversion may not be enough, so we need to improve production efficiency by developing fuel from water and carbon dioxide with biological-inspired nanoscale assemblies, innovative configurations of natural photosynthetic pathways, and genetic engineering to boost biomass production(Moustafa *et al.*, 2021, 2022; Nnannaa *et al.*, 2024; Sharma *et al.*, 2024; Shetti *et al*., 2019). Photovoltaic systems still face a significant challenge in aligning intermittent energy production with fluctuating power demand. To tackle this challenge, an option is to integrate a storage element into these sporadic energy sources.

In two dimensions, dichalcogenides are a versatile group of materials with diverse properties and numerous potential applications. TMDCs have gained popularity following the rise of graphene, the original 2D material made of carbon with semi-metallic properties. Scientists have conducted extensive research on group 6 elements such as molybdenum and tungsten, focusing on their semiconducting sulfides and selenides and their potential applications (Tian *et al.*, 2022; Tripathi *et al*., 2021; Valussi *et al*., 2021; Ye *et al.*, 2023). Recently, attention has shifted to a group of semiconducting materials, namely $HfSe_2$, $ZrSe_2$ HfS_2, and ZrS_2, because of their potential in semiconductor applications. Despite limited studies, both ZrS_2 and HfS_2 are likely indirect band gap semiconductors, regardless of their thickness. The reported band gaps of 1.8–1.7 eV for ZrS_2 and 2.1–1.8 eV for HfS_2 in bulk are suitable for different semiconductor applications.

Tian *et al*. [20] successfully showed the deposition of high-quality, uniform ZrS_2 films on c-plane sapphire substrates using chemical vapor deposition. The atomic interface between ZrS2 and sapphire exhibits an exceptional level of sharpness. ZrS_2 films show optoelectronic applications through photodetector devices. The ZrS_2 photodetectors show exceptional performance, with a light on/off ratio of 106 and a specific directivity of 2.6×10^{12} Jones, which is the highest among other group-IVB two-dimensional Transition-metal dichalcogenides (TMDs). Mattinen *et al* (Mattinen *et al.*, 2019) introduced a method that enables the creation of uniform films on different substrates with precise control over thickness. To increase the process scale, industry-compatible precursors and temperatures around 400 °C can be used. The deposited ZrS_2 and HfS_2 films are smooth, crystalline, with oxygen as the primary impurity. Applying an AlxSiyOz layer in a vacuum environment eliminated ZrS_2 and HfS_2's sensitivity to oxidation and reduced impurities. ZrS_2 and HfS_2photodetectors exhibit exceptional performance, remaining stable even in ambient conditions. The photo-responsively achieved is comparable to ZrS_2 and HfS_2 thin films or single flakes deposited at higher temperatures, but the response speed seems limited by photo-gating, as expected for 2D photo-detectors. The initial atomic layer deposition (ALD) techniques for

ZrS_2 and HfS_2 open up new possibilities for exploring their semiconductor applications.

ZrS doped with silver displays excellent carrier mobility and a large bandgap as a semiconductor. Extensive studies have been carried out to explore its potential applications in optoelectronics, photovoltaics, and sensing. Methods like chemical vapor deposition, molecular beam epitaxy, sol-gel processing, and electrochemical deposition technique (Ikhioya *et al*., 2020; Ikechukwu & Ikhioya, 2024; Ikhioya, 2015b, 2015a; Ikhioya *et al*., 2015, 2020, 2021; Ikhioya and Ekpunobi, 2014b, 2014a; Ikhioya and Nkele, 2023a, 2023b; Ikhioya *et al*., 2023) can synthesize silver-doped ZrS. The doping level and distribution can be controlled by adjusting the synthesis parameters. The addition of silver to ZrS shows promise in photocatalysis, energy storage, and biomedicine. Scientists are investigating how it can be used in flexible electronics and transparent conductors (Alnehia *et al.*, 2023; Sharma *et al.*, 2024; Shetti *et al*., 2019).

The primary aim of this research is to investigate a nanostructured material produced by incorporating silver (Ag) into zirconium sulfide (ZrS). This material exhibits specific attributes and has practical applications in diverse areas. Silver-doped ZrS nanostructures have shown significant potential in optoelectronics, photocatalysis, and energy storage. Their unique optical and electrical properties can be advantageous for solar cells, photodetectors, and batteries.

Experimental Procedures

In this study, we employed the electrochemical deposition technique (ECD). The electrochemical bath system consists of $ZrOCl_2.8H_2O$ (Zr^{2+}) as the cation source, C_2H_5NS (S^{2-}) as the anion source, and distilled water, all combined in a 100-mL beaker. A magnetic stirrer was used to stir the reaction bath. The power supply generated the electric field (DC voltage), with the cathode made of conducting glass and the anode composed of carbon and fluorine electrodes. Uniform thin film deposition through electrochemical deposition has been achieved. The FTO-coated working electrode, measuring 2.5 cm × 1.5 cm, was fragmented and cleaned using dish washing liquid. To synthesize Ag/ZrS, measure 0.01-0.03 mol of $AgNO_3$ precursor, a 0.1 mol $ZrOCl_2.8H_2O$ solution in a 100-mL beaker, and a 0.5 mol C_2H_5NS precursor. The synthesis employs a three-electrode system. The anode is made of platinum, the reference electrode is made of silver and silver chloride (Ag/AgCl), and the cathode is made of FTO (fluorine-doped tin oxide). The FTO-coated substrate housed the counter and reference electrodes vertically in the beaker. The synthesis involved maintaining a potentiostatic condition of -200 mV versus SCE for 5 seconds. The synthesized films were cleaned and dried using a hand dryer. Target materials were poured into beakers alongside equal amounts of precursors during the synthesis process. The films underwent a 20-minute annealing process to remove internal stress. The optical, structural, elemental analysis, and electrical properties of the deposited materials were thoroughly examined using appropriate tools.

Results and Discussion

The structural analysis of silver doped ZrS material.

The undoped zirconium sulphide (ZrS) and Ag/ZrS X-ray diffraction patterns (XRD) at dopant concentrations of 0.01 to 0.03 mol are shown in Figure 1. The ZrS and Ag/ZrS XRD patterns showed the materials are polycrystalline with distinct phase orientation planes. The intense peak, indexed at (101 to 112), represents values from 23.59^o to 62.62^o. It also has a heavily damped peak

plane at (111). The deposited material is appropriate for use in optoelectronics applications. (Chukwuemeka *et al.*, 2024; Emmanuel *et al.*, 2022; Akpu *et al*., 2021; Ikhioya *et al*., 2020; Ikechukwu and Ikhioya, 2024; Ikhioya *et al*., 2020, 2021, 2023;Ikhioya and Ekpunobi, 2014a; Ikhioya and Nkele, 2023b, 2023a; Ikhioya *et al.*, 2023).When silver is incorporated into the ZrS lattice, it facilitates the formation of ZrS crystals. As the 2 theta angle increases, the intensity of X-ray diffraction peaks increases, suggesting more crystallites and larger sizes. The increase in the size of the crystallites in Table 1 is causing the growth due to a decrease in surface energy. The total energy of the system decreases as the crystallites grow, leading to a decrease in the surface area. The addition of silver dopant atoms changes how crystals grow, leading to the formation of bigger crystallites. The larger crystallite size observed at higher 2 theta angles in silver doped ZrS is due to crystal growth caused by reduced surface energy and the impact of silver dopant atoms on growth kinetics. Grain growth causes an increase in the crystallite size of silver-doped ZrS with an increasing 2 theta angle. When the 2theta angle increases, the X-ray beam explores larger crystallites by penetrating deeper into the material. The X-ray diffraction pattern will reveal details about the larger crystallites, leading to increased peak intensity and broader peak width. A wider peak width suggests a greater range of crystal sizes, with the larger crystals causing the higher 2 theta angles. In simpler words, as the X-ray beam goes deeper, it encounters bigger crystallites, causing the crystallite size to increase as the 2 theta angle increases. This phenomenon occurs frequently in materials that demonstrate grain growth, where smaller crystallites combine to create larger ones.

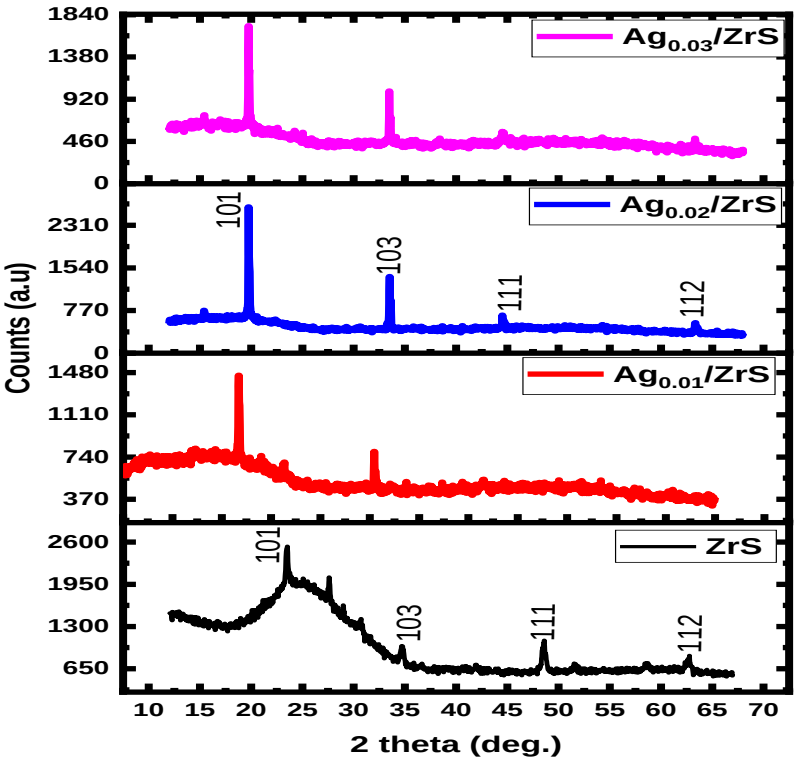

Figure 1: XRD pattern of ZrS and Ag/ZrS

Table 1: Structural parameters of ZrS and Ag/ZrS

Film	2θ (deg.) Recast	d (spacing) Å	(Å)	(β)	(hkl)	(D) nm	**σ** lines/m^2
ZrS	23.5941	3.7672	6.5250	0.2021	101	7.0076	6.2032
	34.9137	2.5674	5.1349	0.2021	103	7.1908	5.8912
	48.4287	1.8778	3.7557	0.2021	111	7.5215	5.3847
	62.6298	1.4819	3.3136	0.2021	112	8.0295	4.7250
$Ag_{0.01}$/ZrS	19.6836	4.5059	7.8046	0.2032	101	6.9251	6.3518
	33.8347	2.6468	5.2936	0.2032	103	7.1318	5.9890
	44.5183	2.0332	4.0665	0.2032	111	7.3727	5.6042
	63.3158	1.4674	3.2814	0.2032	112	8.0163	4.7406
$Ag_{0.02}$/ZrS	19.6836	4.5059	7.8046	0.2235	101	6.2961	7.6843
	33.8347	2.6468	5.2936	0.2235	103	6.4841	7.2453
	44.5183	2.0332	4.0665	0.2235	111	6.7031	6.7798
	63.3158	1.4674	3.2814	0.2235	112	7.2882	5.7351
$Ag_{0.03}$/ZrS	19.6836	4.5059	7.8046	0.2300	101	6.1182	8.1377
	33.8347	2.6468	5.2936	0.2300	103	6.3009	7.6728
	44.5183	2.0332	4.0665	0.2300	111	6.5136	7.1798
	63.3158	1.4674	3.2814	0.2300	112	7.0823	6.0735

Scanning electron microscopy (SEM) of ZrS and Ag/ZrS

Figure 2 displays the microstructure of Ag/ZrS. The micrograph of the ZrS material shows a presence of hexagonal structure material along with precipitate. The presence of various silver concentrations results in particle clumping and a uniformly coated substrate surface. The contact between the chalcogenide material and transition metal results in the formation of silver precipitate, and ZrS exhibits visible indications of material sublimation. SEM micrographs reveal the formation of diversely shaped nanoparticles, a consequence of the Ag/ZrS reaction. The synthesized material, at a quantity of 0.01 mol, illustrates the transformation of the silver precipitate by the dopant, showing compatibility between the two materials. However, increasing the dopant molarity to (0.02 mol) caused the nanoparticles to restructure, showing that exceeding (0.03 mol) would cause material reversal. The XRD findings show that the rise in silver molarity directly correlates with the growth of crystallite size. The results show that film syntheses hold promise for solar cell and photovoltaic use. Figure 3 shows the elemental dispersive X-ray (EDXs) analyzes of the material. Zirconium, sulfur, and silver are the basic elements showed by the spectra.

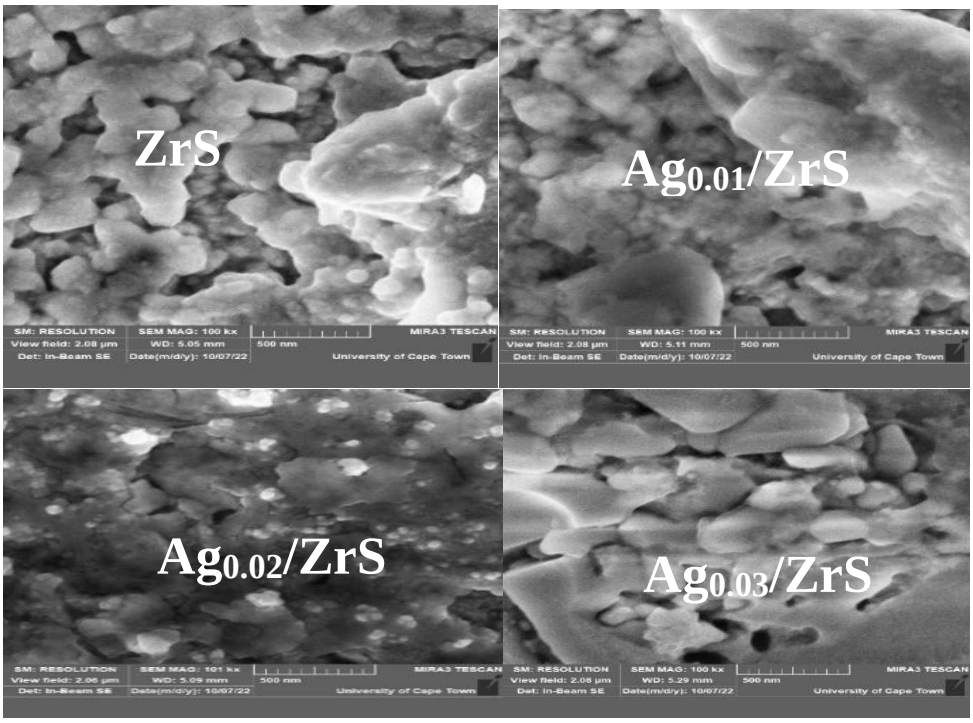

Figure 2: SEM micrograph of ZrS and Ag/ZrS

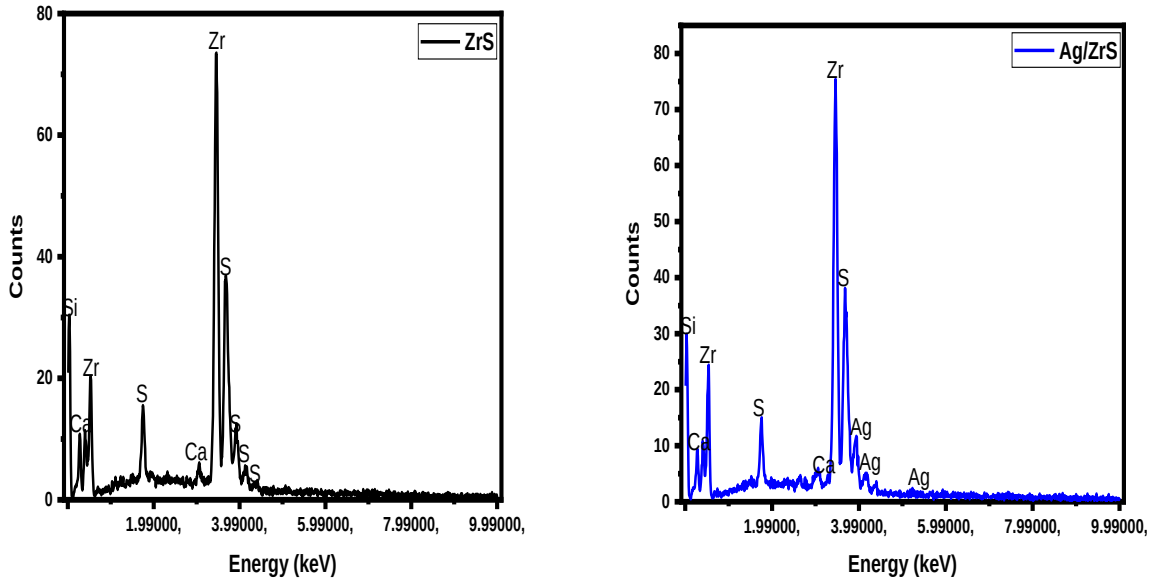

Figure 3: EDXs spectrum of ZrS and Ag/ZrS

Optical analysis of ZrS and Ag/ZrS

The absorbance of Ag/ZrS is shown in Figure 4 (a). As the wavelength of the films increases, the material's absorbance decreases. In the visible region, the Ag/ZrS material displays a distinct absorption band, which is attributed to the silver surface plasmon resonance. The wavelength of the surface plasmon resonance band is

determined by the size, shape, and dielectric properties of the silver material and the surrounding ZrS material. Analyzing the absorption spectra allows for determining the properties of Ag/ZrS material, such as silver size and shape, ZrS dielectric properties, and material interaction. Ag/ZrS material finds applications in various fields like photocatalysis, solar cells, and sensors (Malumi *et al.*, 2023; Ojegu, Odia, *et al.*, 2023; Ojegu, Samuel, *et al.*, 2023; Okeoghene *et al.*, 2023; Rufus *et al.*, 2023; Samuel, Ojoba, *et al.*, 2023; Samuel, *et al.*, 2023; Sarwar *et al.*, 2023; Shah *et al.*, 2023; Udofia *et al.*, 2023; Udofia and Ikhioya, 2018). By examining the absorption spectra of Ag/ZrS material, its optical characteristics improve its functionality for specific uses. Figure 4 (b) displays the transmittance of Ag/ZrS. The material's transmittance increases as the wavelength of the films increases. The transmittance spectral measure the amount of light passing through a material at different wavelengths. By using this data, the material exhibits the properties for specific applications, such as optoelectronics or energy storage. The transmittance spectra of Ag/ZrS can design optoelectronic devices, such as solar cells, light emitting diodes (LEDs), and photodetectors. The efficiency and performance of these devices enhanced by customizing their optical properties. Figure 4 (c) displays the reflectance of Ag/ZrS. The material's reflectance decreases as the films' light radiation increases. The wavelength of incident light has a significant impact on the reflectance spectra of Ag/ZrS material. Ag/ZrS has strong reflectance in the visible region but decreases significantly in the near-infrared region. The plasmonic resonance of silver in the Ag/ZrS composite is responsible for the behavior. The reflectance spectra of Ag/ZrS altered by manipulating the size and shape of silver. Smaller silver materials cause the plasmonic resonance peak to shift towards the blue end. The tunability of Ag/ZrS materials allows for designing specific optical properties for various applications. The application of Ag/ZrS materials with reflectance that varies with wavelength is versatile, spanning areas like photocatalysis, sensing, and optical devices. Ag/ZrS shows great potential for solar energy collection because it reflects light well in the visible region and has low reflectance in the near-infrared region, making it suitable for stealth technology. Figure 4 (d) displays the bandgap of Ag/ZrS. The Ag/ZrS material has a direct band gap at the UV point, making it ideal for optoelectronic applications. Efficient light emission happens when the valence band maximum and conduction band minimum align at the same k-point. The optoelectronic characteristics of Ag/ZrS material can be customized by varying the amount of Ag. By adjusting the Ag concentration, specific optical features can be achieved for different applications, altering the bandgap. The Ag/ZrS material has potential in optoelectronic applications as LEDs, photodetectors, and solar cells. Its potential to change its bandgap and efficient radiative recombination makes it a promising option for future optoelectronic devices(Kashif *et al.*, 2022). By incorporating silver into the ZrS lattice, the energy band structure rises from 2.32 to 2.51 eV as molarity increases.

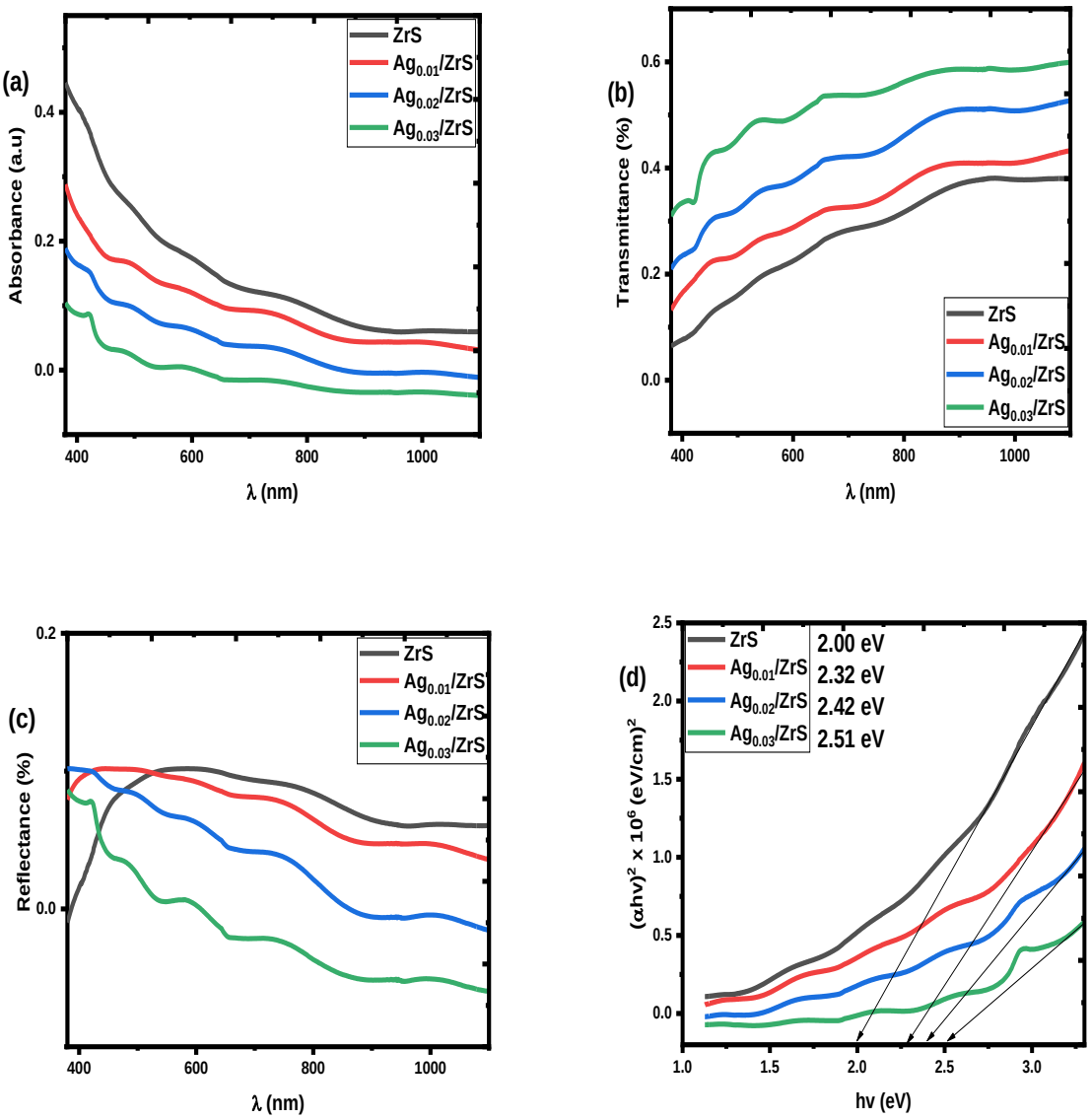

Figure 4: absorbance (a), transmittance (b), reflectance (c), and bandgap (d) of ZrS and Ag/ZrS

The refractive index of Ag/ZrS is illustrated in Figure 5 (a). As the photon energy of the material rises, the refractive index fluctuates. The refractive index spectra of Ag/ZrS material have important implications for its applications. For instance, in optoelectronics, the material's refractive index influences the performance of optical devices, such as lenses, prisms, and wave guides. Figure 5 (b) shows the extinction coefficient of Ag/ZrS. The increase in photon energy leads to an increase in the extinction coefficient of the material. The extinction coefficient quantifies how well a material can absorb and scatter light. By examining the spectra, scientists can learn about the material's uses in optoelectronics and other areas. Optimizing devices that use the optical properties of Ag/ZrS requires a thorough understanding of its extinction coefficient

spectra. The optical conductivity of Ag/ZrS is depicted in Figure 5 (c). As the photon energy rises, so does the material's optical conductivity. The optical conductivity spectra of Ag/ZrS show a clear dependence on photon energy. At low photon energies, the optical conductivity is dominated by intra-band transitions within the valence band. As the photon energy increases, inter-band transitions from the valence band to the conduction band become more significant, leading to a sharp increase in the optical conductivity. The optical conductivity of Ag/ZrS material increases with increasing photon energy. This is due to the increasing number of inter-band transitions that are possible in higher photon energies. The optical conductivity also shows a peak at around 2.3 eV, which corresponds to the bandgap of Ag/ZrS material. The optical conductivity spectra of Ag/ZrS material study the electronic structure and optical properties of the material. Figure 5 (d&e) shows the dielectric constant (both real and imaginary parts) of Ag/ZrS. The real and imaginary dielectric constant of the material increases as the photon energy increases. The real dielectric constant measures a material's ability to store electrical energy, while the imaginary dielectric constant quantifies energy loss from polarization. Valuable information about the optical properties of Ag/ZrS material can be obtained by analyzing the photon energy spectra of these constants. The dielectric constant of Ag/ZrS material increases with higher photon energy. The material becomes more polarizable as the energy levels rise. As photon energy increases, the dielectric constant of Ag/ZrS material varies. At higher energies, the material encounters less energy loss due to polarization.

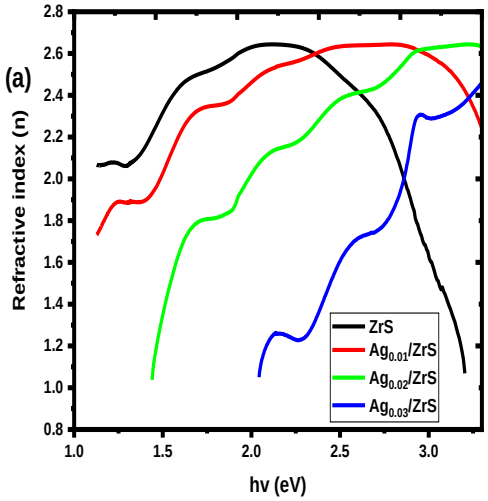

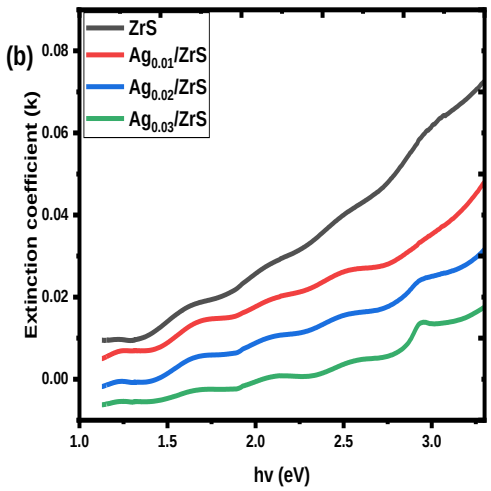

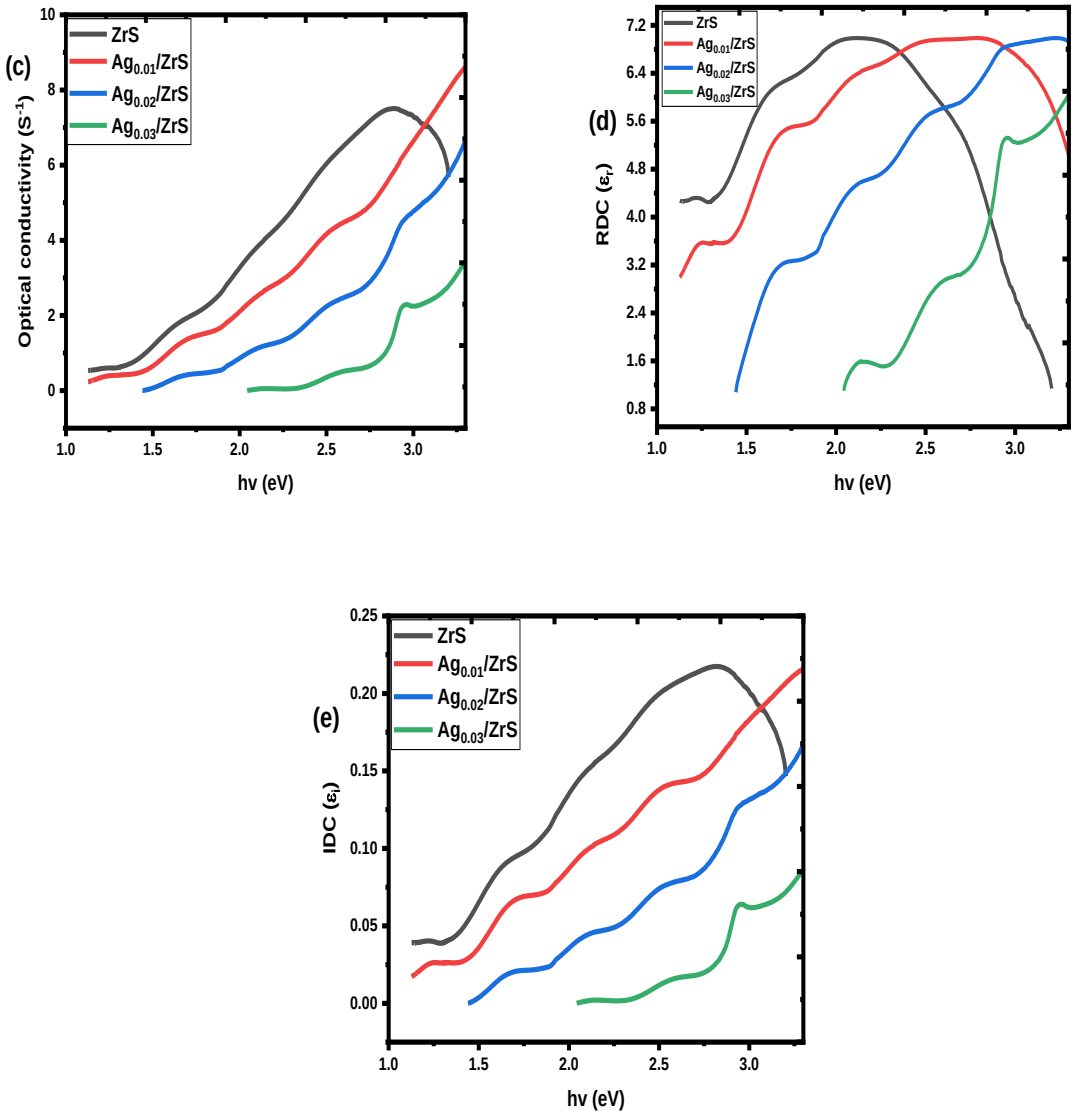

Figure 5: refractive index (a), extinction coefficient (b), optical conductivity (c), real dielectric constant (RDC) (d), imaginary dielectric constant (IDC) (e) of ZrS and Ag/ZrS

The electrical analysis of ZrS and Ag/ZrS

The resistivity and conductivity of ZrS and Ag/ZrS material are shown in Table 2. Increasing the film thickness from 121.32 to 129.04 nm resulted in a decrease in resistivity from 2.36 to 3.56 ohm/m and a drop in conductivity from 4.34 to 2.80 S/m. The films' low resistivity and conductivity make them perfect for photovoltaic and solar cell applications. Figure 6 shows that as film thickness increases, resistivity decreases and conductivity increases. The graph shows the lack of an ohmic relationship between resistivity, conductivity, and silver molarity.The plot illustrates how film thickness, resistivity, conductivity, and silver molarity fluctuations are interconnected.

Table 2: Electrical properties of ZrS and Ag/ZrS

Film	t (nm)	ρ (Ω.m)	σ $(S/m)^{-1}$
ZrS	121.32	2.36×10^6	4.34×10^5
$Ag_{0.01}$/ZrS	123.04	3.23×10^6	3.09×10^5
$Ag_{0.02}$/ZrS	126.13	3.43×10^6	2.91×10^5
$Ag_{0.03}$/ZrS	129.04	3.56×10^6	2.80×10^5

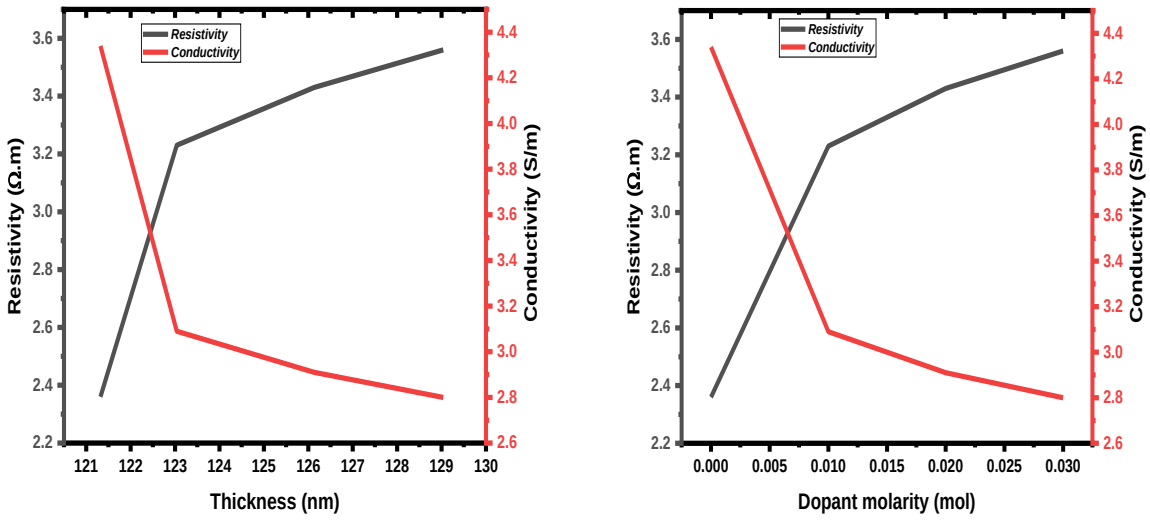

Figure 6: variation of resistivity and conductivity of ZrS and Ag/ZrS

Conclusions

The successful utilization of the electrochemical deposition technique allowed for the synthesis and study of Ag/ZrS thin films. The XRD patterns of ZrS and ZrS/Ag indicated the materials are polycrystalline and have well-defined phase orientation planes. Increasing the 2 theta angle leads to stronger X-ray diffraction peaks, suggesting larger crystallites and greater crystallinity. Reduced surface energy drives the growth of the crystallites, as they increase in size. As the crystallites increase in size, the total energy of the system diminishes, resulting in a reduced surface area. Silver dopant atoms affect the way crystals grow, resulting in larger crystallites. The increased crystallite size observed at higher 2 theta angles in silver-doped ZrS can be attributed to crystal growth, facilitated by lower surface energy and the impact of silver dopant atoms on growth kinetics. The resistivity dropped from 2.36 to 3.56 ohm/m as the film's thickness increased from 121.32 to 129.04 nm, resulting in a decrease in conductivity from 4.34 to 2.80 S/m. The films' low resistivity and conductivity make them perfect for photovoltaic and solar cell applications. By incorporating silver into the ZrS lattice, the energy band structure rises from 2.32 to 2.51 eV as molarity increases.

Acknowledgment

We express our gratitude to the authors for their significant financial support, which played a vital role in the research's success.

Author contribution statement

Shaka O. Samuel, Imosobomeh L. Ikhioya: methodology, conceptualization, data curation, data collection, **Olisenekwu Cletus, Imosobomeh L. Ikhioya:** samples characterization, first-draft writing, software, reviewing, and editing**. Imosobomeh L. Ikhioya, Shaka O. Samuel:** supervisor, investigation and visualization**.** All authors approved the submission of the manuscript.

Disclosing conflicting interests.

The authors of this paper declare that there are no personal or financial conflicts that may have affected the study.

Availability of data

Access to the data is available upon request.

Reference

Alnehia, A., Al-Sharabi, A., Al-Hammadi, A. H., Al-Odayni, A. B., Saeed, W. S., & Alrahlah, A. (2023). Structural, Optical, and Bioactivity Properties of Silver-Doped Zinc Sulfide Nanoparticles Synthesized Using Plectranthus barbatus Leaf Extract. *Journal of Chemistry*, *2023*. https://doi.org/10.1155/2023/1399703

Alzoubi, T., Moghrabi, A., Moustafa, M., and Yasin, S. (2021). Efficiency boost of CZTS solar cells based on double-absorber architecture : Device modeling and analysis. *Solar Energy*, *225*(July), 44–52. https://doi.org/10.1016/j.solener.2021.07.012

Bencherif, H., Dehimi, L., Mahsar, N., Kouriche, E., and Pezzimenti, F. (2022). Materials Science & Engineering B Modeling and optimization of CZTS kesterite solar cells using TiO 2 as efficient electron transport layer. *Materials Science & Engineering B*, *276*(April 2021), 115574. https://doi.org/10.1016/j.mseb.2021.115574

Bouarissa, A., Gueddim, A., Bouarissa, N., and Maghraoui-meherezi, H. (2021). Materials Science & Engineering B Modeling of ZnO / MoS 2 / CZTS photovoltaic solar cell through window , buffer and absorber layers optimization. *Materials Science & Engineering B*, *263*(September 2020), 114816. https://doi.org/10.1016/j.mseb.2020.114816

Chukwuemeka, E. J., Osita, N. A., Odira, A. O., Uchechukwu, U. C., Mimi, J. D., and Ikhioya, I. L. (2024). Performance and Stability Evaluation of Low-Cost Inorganic Methyl Ammonium Lead Iodide (CH3NH3PbI3) Perovskite Solar Cells Enhanced with Natural Dyes from Cashew and Mango Leaves. *Advanced Journal of Chemistry, Section A*, *7*(1), 27–40. https://doi.org/10.48309/ajca.2024.406961.1384

Elhalim, A., Abderrezek, M., and Elamine, M. (2021). Optik Numerical study of CZTS / CZTSSe tandem thin film solar cell using. *International Journal for Light and Electron Optics 242* (May), 167320. https://doi.org/10.1016/j.ijleo.2021.167320

Emmanuel, O. C., Donald, O. N., and Ikhioya, I. L (2022). Effect of Doping and Co-sensitization on the Photovoltaic Properties of Natural Dye-sensitized Solar Cells. *International Journal of Applied Physics*, *9*(3), 44–54. https://doi.org/10.14445/23500301/ijap

-v9i3p105

Agbim, E. G, Ikhioya, I. L and Ekpunobi A. J. (2019). Syntheses And Characterization Of Fluorine Doped Tin Oxide Using Spray Pyrolysis Technique . *IOSR Journal of Applied Physics (IOSR - JAP)*, *11*(3), 70–78. https://doi.org/10.9790/4861-1103017078

Hasan, S., Ahmed, M. T., Roman, A. Al, Islam, S., and Ahmed, F. (2023). Investigation of Structural, Electronic, and Optical Properties of Chalcogen-Doped ZrS2: A DFT Analysis. *Advances in Materials Science and Engineering*, *2023*. https://doi.org/10.1155/2023/6525507

Akpu N. I., Asiegbu A.D, Nnanna L. A, Ikhioya I. L, (2021) "Investigation On The Influence of Varying Substrate Temperature On The Physical Features of Yttrium Doped Cadmium Selenide Thin Films Materials," *SSRG International Journal of Applied Physics*, vol. 8, no. 2, pp. 37-46, 2021. https://doi.org/10.14445/23500301/IJAP-V8I2P106

Ikhioya I. L, Chigozirim, E., Doris O, O., C. Rita, A., and C. Ogonnaya, O. (2020). The Influence of Precursor Temperature on The Properties of Erbium-Doped Zirconium Telluride Thin Film Material Via Electrochemical Deposition. *International Journal of Applied Physics*, *7*(1), 102–109. https://doi.org/10.14445/23500301/ijap-v7i1p115

Ikechukwu, O., and Ikhioya, I. L. (2024). *Effect of Sodium Arsenic on the Improvement of TiO 2 / Dye as Photosensitizers in Dye-Sensitized Solar Cells (DSSC). Asian Journal of Green Chemistry Original Research 8*, 137–149. https://doi.org/10.48309/ajgc.2024.419357.1451

Ikhioya, I. L. (2015a). Characterization of zinc sulphide thin film prepared by electrodeposition method. *International Journal of ChemTech Research*, *8*(2), 655–660.

Ikhioya, I. L. (2015b). Research in Chemistry and Environment Optical and Electrical Properties of Copper Telluride Thin Films. *International Journal for Research in Applied and Natural Science*, *5*(3), 28–32.

Ikhioya, I. L. (2024). *Enhanced Structural, Morphological and Optical Features of Ti. 4*, 195–207.

Ikhioya, I. L., Akpu, N. I., and Nkele, A. C. (2021). Influence of ytterbium (Yb) dopant on the optical properties of electrochemically deposited zinc oxide (ZnO) films. *Materials Research Express*, *8*(1), 16–18. https://doi.org/10.1088/2053-1591/abd5d6

Ikhioya, I. L., and Ekpunobi, A. J. (2014a). Effect of Deposition Period and pH on Electrodeposition Technique of Zinc Selenide Thin Films Materials and Methods Results and Discussion Optical Properties of ZnSe Films. *Journal of the Nigerian Association of Mathematical Physics*, *28*(2), 281–288.

Ikhioya, I. L., and Ekpunobi, A. J. (2014b). The Optical Properties of CdSe / ZnSe Superlattice by Electrodeposition Technique The Optical Properties of CdSe / ZnSe … Ikhioya and Ekpunobi J of NAMP. *Journal of the Nigerian Association of Mathematical Physics*, *28*(2), 289–296.

Ikhioya, I. L., and Nkele, A. C. (2023a). A Novel Synthesis of Hydrothermally Prepared Europium Sulfide and Cerium Sulfide Nanomaterials Doped with Yttrium. *Arabian Journal for Science and Engineering*. https://doi.org/10.1007/s13369-023-08292-9

Ikhioya, I. L., and Nkele, A. C. (2023b). Properties of electrochemically deposited NiTe films prepared at varying dopant concentrations of molybdenum. *Journal of Materials Science: Materials in Electronics*, *34*(21). https://doi.org/10.1007/s10854-023-11018-0

Ikhioya, I. L., and Nkele, A. C. (2024). Green synthesis and characterization of aluminum oxide nanoparticle using neem leaf extract (Azadirachta Indica). *Hybrid Advances*, *5*(November 2023), 100141. https://doi.org/10.1016/j.hybadv.2024.100141

Ikhioya, I. L., Nkele, A. C., Ezema, S. N., Maaza, M., and Ezema, F. (2020). A study on the effects of varying concentrations on the properties of ytterbium-doped cobalt selenide thin films. *Optical Materials*, *101*. https://doi.org/10.1016/j.optmat.2020.109731

Ikhioya, I. L., Nkele, A. C., and Ochai-Ejeh, F. U. (2023). Green synthesis of copper oxide nanoparticles using neem leaf extract (Azadirachta indica) for energy storage applications. *Materials Research Innovations*, *00*(00), 1–7. https://doi.org/10.1080/14328917.2023.2252677

Ikhioya, I. L., Okanigbuan, P. N., Agbakwuru, C. B., and Osolobri, B. U. (2015). Journal of the Nigerian Association of Mathematical Physics © J . of NAMP Characterization of Zinc Sulphide / Cadmium Sulphide (ZnS / CdS) Superlattice by Electrodeposition Technique of Physics and Industrial Physics , Nnamdi Azikiwe University , Awka ,. *Journal of the Nigerian Association of Mathematical Physics*, *29*, 331–338.

Ikhioya, I. mosobomeh L., Akpu, N. I., Onoh, E. U., Aisida, S. O., Ahmad, I., Maaza, M., and Ezema, F. I. (2023). Enhanced physical properties of nickel telluride metal chalcogenide material with molybdenum dopant. *Materials Research Innovations*, *00*(00), 1–9. https://doi.org/10.1080/14328917.2023.2222465

Jimin Shang, J. S., Shuai Zhang, S. Z., Yongqiang Wang, Y. W., Hongyu Wen, H. W., and Zhongming Wei, Z. W. (2019). Electronic and optical properties of an intrinsic type-I band alignment ZrS2/SnS2 van der Waals heterostructure for optoelectronic devices. *Chinese Optics Letters*, *17*(2), 020010. https://doi.org/10.3788/col201917.020010

Kashif, M., Anjum, N., Shahzad, A., Rasheed, A., Imran, M., and Manzoor, A. (2022). Tuning the Electronic and Optical Properties of the ZrS2/PtS2van der Waals Heterostructure by an External Electric Field and Vertical Strain. *ACS Omega*, *7*(37), 33453–33460. https://doi.org/10.1021/acsomega.2c04207

Kumar, P., Sharma, V., Kumar, A., Sachdev, K., and Asokan, K. (2016). *Structural, morphological and vibrational properties of Fe 2 O 3 nanoparticles* . *Macromolecular*. *2*(1), 163–163.

https://doi.org/10.3850/978-981-09-7519-7nbl16-rps-163

Li, L., Lv, R., Wang, J., Chen, Z., Wang, H., Liu, S., Ren, W., Liu, W., and Wang, Y. (2019). Optical nonlinearity of ZrS 2 and applications in fiber laser. *Nanomaterials*, *9*(3). https://doi.org/10.3390/nano9030315

Malumi, S. O., Malumi, T., Osiele, M. O., Ekpekpo, A., and Ikhioya, I. L. (2023). Enhance and Performance Evolution of Silver-Doped Titanium Dioxide Dye-Sensitized Solar Cells Using Different Dyes. *Journal of Engineering in Industrial Research*, *4*(4), 189-200. doi: 10.48309/jeires.2023.4.1

Mattinen, M., Popov, G., Vehkamäki, M., King, P. J., Mizohata, K., Jalkanen, P., Räisänen, J., Leskelä, M., and Ritala, M. (2019). Atomic Layer Deposition of Emerging 2D Semiconductors, HfS2 and ZrS2, for Optoelectronics. *Chemistry of Materials*, *31*(15), 5713–5724. https://doi.org/10.1021/acs.chemmater.9b01688

Moustafa, M., Al Zoubi, T., and Yasin, S. (2022). Exploration of CZTS-based solar using the ZrS2 as a novel buffer layer by SCAPS simulation. *Optical Materials*, *124*(January), 112001. https://doi.org/10.1016/j.optmat.2022.112001

Moustafa, M., Zoubi, T. Al, and Yasin, S. (2021). Optik Numerical analysis of the role of p-MoSe 2 interfacial layer in CZTSe thin-film solar cells using SCAPS simulation. *International Journal for Light and Electron Optics 247*(August), 167885. https://doi.org/10.1016/j.ijleo.2021.167885

Nnannaa, L. A., Jospeh, U., Nwaokorongwu, E. C., Ezere, U. A., Akpu, N. I., and Ikhioya, I. L. (2024). Impact of annealing temperature on praseodymium cerium telluride nanoparticles synthesise via hydrothermal approach for optoelectronic application. *Materials Research Innovations*, *00*(00), 1–11. https://doi.org/10.1080/14328917.2024.2320982

Ojegu, E. O., Odia, O. B., Osiele, M. O., Godfrey, A. E., and Ikhioya, I. L. (2023). *Effect of precursor temperature on electrochemically deposited zirconium doped chromium telluride using a standard three-electrode system. Journal of Materials and Environmental Science14*(11), 1148–1159.

Ojegu, E. O., Samuel, S. O., Osiele, M. O., Akpojotor, G. E., and Ikhioya, I. L. (2023). Optimisation of deposition voltage of zirconium-doped chromium telluride via typical three-electrode cell electrochemical deposition technique. *Materials Research Innovations*, *00*(00), 1–9. https://doi.org/10.1080/14328917.2023.2243063

Okeoghene Blessing, I., Shah, H., Afzal, S., and Ikhioya, I. L. (2023). Enhanced structural properties of electrochemically synthesised NiFeS using 500 keV carbon C++ ions irradiation. *Materials Research Innovations*, *00*(00), 1–12. https://doi.org/10.1080/14328917.2023.2262315

Rufus, I., Peter, A., Aisida, S. O., and Ikhioya, I. L. (2023). Results in Optics Influence of manganese molarity incorporation on manganese silver sulphide semiconductor material for photovoltaic applications. *Results in*

Optics, *12*(February), 100464. https://doi.org/10.1016/j.rio.2023.100464

Samuel, S. O., Frank, M. L. E., Ogherohwo, E. P., Ekpekpo, A., Zhimwang, J. T., and Ikhioya, I. L. (2023). Influence of Deposition Voltage on Strontium Sulphide Doped Silver for Optoelectronic Application. *East European Journal of Physics*, *2023*(1), 189–196. https://doi.org/10.26565/2312-4334-2023-1-25

Samuel, S. O., James, F. E., and Ikhioya, I. L. (2023). Effect of dopant on the energy bandgap on strontium sulphide doped silver for optoelectronic application. *Materials Research Innovations*, *00*(00), 1–11. https://doi.org/10.1080/14328917.2023.2212944

Samuel, S. O., Lagbegha-ebi, M. F., Ogherohwo, E. P., and Ikhioya, I. L. (2023). Improve physical properties of zirconium doped strontium sulphide for optoelectronic purpose. *Results in Optics*, *13*(June), 100518. https://doi.org/10.1016/j.rio.2023.100518

Samuel, S. O., Ojoba, C. K., Ogherohwo, E. P., Ojegu, E. O., Zhimwang, J. T., Ekpekpo, A., and Ikhioya, I. L. (2023). The influence of precursor temperature on strontium sulphide doped silver for optoelectronic application. *Journal of the Indian Chemical Society*, *100*(5), 100992. https://doi.org/10.1016/j.jics.2023.100992

Samuel, S. O., Timothy, Z. J., Ojoba, C. K., and Ikhioya, I. L. (2023). Temperature's Impact on the Physical Properties of Rare Earth Element Doped SrS for Optoelectronic Use. *Journal of Engineering in Industrial Research*, *4*(3), 147-156. doi: 10.48309/jeires.2023.3.2

Sarwar, S. G., Ikhioya, I. L., Afzal, S., and Ahmad, I. (2023). Supercapitance performance evaluation of MXene/Graphene/NiO composite electrode via in situ precipitation technique. *Hybrid Advances*, *4*, 100105. https://doi.org/10.1016/j.hybadv.2023.100105

Shah, H., Afzal, S., Usman, M., Shahzad, K., and Ikhioya, I. L. (2023). Impact of Annealing Temperature on Lanthanum Erbium Telluride (La0.1Er0.2Te0.2) Nanoparticles Synthesized via Hydrothermal Approach. *Advanced Journal of Chemistry, Section A*, *6*(4), 342–351. https://doi.org/10.22034/AJCA.2023.407424.1386

Sharma, C. P., Gupta, A., Khadka, M., Ben-Yoav, H., Ronen, A., and Arnusch, C. J. (2024). Silver nanoparticle doped laser-induced graphene fabrication methodology affects silver nanoparticle size, distribution, biological and electrochemical properties. *Environmental Science: Nano*. https://doi.org/10.1039/d3en00371j

Shetti, N. P., Malode, S. J., Nayak, D. S., Aminabhavi, T. M., and Reddy, K. R. (2019). Nanostructured silver doped TiO2/CNTs hybrid as an efficient electrochemical sensor for detection of anti-inflammatory drug, cetirizine. *Microchemical Journal*, *150*. https://doi.org/10.1016/j.microc.2019.104124

Tian, Y., Cheng, Y., Huang, J., Zhang, S., Dong, H., Wang, G., Chen, J., Wu, J.,

Yin, Z., and Zhang, X. (2022). Epitaxial growth of large area ZrS2 2D semiconductor films on sapphire for optoelectronics. *Nano Research*, *15*(7), 6628–6635. https://doi.org/10.1007/s12274-022-4308-4

Tripathi, S., Kumar, B., and Dwivedi, D. K. (2021). Optik Numerical simulation of non-toxic In 2 S 3 / SnS 2 buffer layer to enhance CZTS solar cells efficiency by optimizing device parameters. *International Journal for Light and Electron Optics 227*(August 2020), 166087. https://doi.org/10.1016/j.ijleo.2020.166087

Udofia, K. I., Ikhioya, I. L., Okoli, D. N., and Azubike, J. (2023). *Asian Journal of Nanoscience and Original Research Article Impact of doping on the physical properties of PbSe chalcogenide material for photovoltaic application*. *2*, 135–147. https://doi.org/10.26655/AJNANOMAT.2023.2.3

Udofia, K., and Ikhioya, I.L (2018). Electrical Properties of Electrodeposited Lead Selenide (PbSe) Thin Films. *Asian Journal of Physical and Chemical Sciences*, *5*(4), 1–7. https://doi.org/10.9734/ajopacs/2018/40383

Valussi, M., Antonelli, M., Donelli, D., and Firenzuoli, F. (2021). Jo l P of. *Perspectives in Medicine*, 100451. https://doi.org/10.1016/j.hybadv.2024.100170

Ye, L., Luan, L., Guo, R., Zhang, Y., Wei, X., Fan, J., Ni, L., Liu, C., Yang, Y., Liu, J., Tian, Y., and Duan, L. (2023). Optical and tunable electronic properties of doped PtS2/ZrS2 Van Der Waals heterostructure under the effect of strain and electric field. *Materials Science in Semiconductor Processing*, *164*(March), 107615. https://doi.org/10.1016/j.mssp.2023.107615